AIAA JOURNAL
Vol. 43, No. 1, January 2005

Ninety-Degree Acoustic Spectrum of a High-Speed Air Jet

M. E. Goldstein*
NASA John H. Glenn Research Center at Lewis Field, Cleveland, Ohio 44135

Tam and Auriault successfully predicted the acoustic spectrum at 90 deg to the axis of a high-speed air jet by using an acoustic equation derived from ad hoc kinetic theory-type arguments. It is shown that similar predictions can be obtained by using a rigorous acoustic analogy approach together with actual measurements of the relevant acoustic source correlations. This puts the result on a firmer basis and enables its extension to new situations and to the prediction of sound at other observation angles.

I. Introduction

THE prediction of aircraft exhaust noise continues to be a fruitful area of research. Computational demands still preclude the use of full-scale direct numerical simulation (or even large-eddy simulation[1]) at the high Reynolds numbers and complex geometries of practical interest, and the current emphasis remains focused on developing acoustic-analogy type approaches in which the Navier–Stokes equations are rearranged into a form that separates out the linear terms and associates them with propagation effects that can then be determined as part of the calculation. The nonlinear terms are treated as known source functions to be determined by modeling and, in more recent approaches, parameterized with the parameters being determined from a steady Reynolds averaged Navier–Stokes (RANS) calculation. The base flow (about which the linearization is carried out) is usually assumed to be parallel, and the resulting equation is usually referred to as Lilley's[2] equation.

Most of the early approaches, including the original Mani–Gliebe–Balsa (MGB) (see Ref. 3) approach, which neglect variations in retarded time in an appropriate moving frame coordinate system and assume the resulting moving frame correlation tensor to be separable into the product of (usually Gaussian) temporal and spatial components, significantly overpredict both the high- and low-frequency rolloff of the 90-deg acoustic spectrum.[4] Tam and Auriault[5] achieved much greater success in this endeavor by using ad hoc kinetic theory-type arguments to derive their acoustic equation. However, Morris and Farassat[4] later showed that their result is equivalent to the usual acoustic-analogy approach (at least in so far as its predictions of the 90-deg spectrum are concerned) with the primary difference being in the modeling of the source term, which amounts to assuming a (nonseparable) functional form for the second convective derivative of the turbulence correlation that is similar to the functional form used for the turbulence correlation itself in the usual acoustic-analogy approaches; however, see Refs. 6 and 7. Unfortunately, this forces the resulting turbulence spectrum to be singular and, therefore, incompatible with experimental observations, which would certainly be undesirable in any physics-based theory.

The main purpose of this paper is to show that the Tam and Auriault[5] spectrum can be recovered from an acoustic-analogy approach that uses experimentally based, that is, physically realizable, source modeling together with an appropriate acoustic analogy equation. In Ref. 8, it is shown that the Navier–Stokes equations can always be rearranged into the form of the linearized Navier–Stokes equations about a very general base flow, but with nonlinear dependent variables, with the viscous stresses replaced by a generalized Reynolds stress and with the heat flux vector replaced by a generalized stagnation enthalpy flux (which would be treated as known source strengths when the generalized equations are used as the bases for an acoustic-analogy approach). This result leads to a form of Lilley's[2] equation with modified source term when the base flow is taken to be a unidirectional transversely sheared mean flow, that is, a parallel flow.

It is generally agreed that the stagnation enthalpy fluxes, which correspond to the isentropic part of the pressure density source in the Lighthill approach (see Ref. 2) are only important for hot jets[2,9–11] except, perhaps, at small angles to the downstream jet axis.[12] They are, therefore, neglected in the present analysis. The resulting equation is solved using a more or less conventional Greens function approach, and the solution is then used to calculate the far-field acoustic spectrum. Neglect of the enthalpy and viscous sources are the only approximations introduced at this stage of the analysis, but the results are then simplified by first neglecting variations in retarded time (in an appropriate moving coordinate system[13]) and then introducing an axisymmetric turbulence model.[14–19] Finally, an empirical turbulent source spectrum, based on recent measurements of Harper-Bourne[20] (in a low Mach number jet), is incorporated into the result, and it is shown that the predicted far-field acoustic spectrum at 90 deg to the jet axis is essentially the same as the one proposed by Tam and Auriault.[5]

II. Acoustic-Analogy Equation and Its Far-Field Solution

It is shown in Ref. 8 that the Navier–Stokes equations can be rewritten (for an ideal gas) as the linearized Navier–Stokes equations about a very general base flow but with different (in general nonlinear) dependent variables, with the heat flux vector replaced by a generalized enthalpy flux and with the viscous stresses replaced by a generalized Reynolds stress. This is a true acoustic analogy (in the Lighthill[21,22] sense) in that it shows that there is an exact analogy between the flow fluctuations in any real flow and the linear fluctuations about a very general base flow due to an externally imposed viscous stress and heat flux vector. When the base flow is taken to be the unidirectional transversely sheared mean flow,

$$v_i = \delta_{i1} U(x_2, x_3), \qquad \rho = \bar{\rho}(x_2, x_3), \qquad p = \bar{p} = \text{const} \quad (1)$$

where $\boldsymbol{x} = \{x_1, x_2, x_3\}$ is a Cartesian coordinate system, $\boldsymbol{v} = \{v_1, v_2, v_3\}$ is the velocity, p is the pressure, and ρ is the density, the general equations reduce to the modified Lilley's[2] equation

$$Lp'_e = \frac{\mathrm{D}}{\mathrm{D}t}\left(\frac{\partial}{\partial x_i}\widetilde{c^2}\frac{\partial e'_{ij}}{\partial x_j}\right) - \frac{\partial U}{\partial x_i}\left(2\widetilde{c^2}\frac{\partial^2 e'_{ij}}{\partial x_1 \partial x_j} + (\gamma - 1)\frac{\mathrm{D}^2}{\mathrm{D}t^2}e'_{1i}\right)$$

$$- (\gamma - 1)\frac{\mathrm{D}^2}{\mathrm{D}t^2}\frac{\partial \eta'_j}{\partial x_j} \quad (2)$$

where

$$L \equiv \frac{\mathrm{D}}{\mathrm{D}t}\left(\frac{\partial}{\partial x_i}\widetilde{c^2}\frac{\partial}{\partial x_i} - \frac{\mathrm{D}^2}{\mathrm{D}t^2}\right) - 2\frac{\partial U}{\partial x_j}\frac{\partial}{\partial x_1}\widetilde{c^2}\frac{\partial}{\partial x_j} \quad (3)$$

Received 13 March 2004; revision received 14 June 2004; accepted for publication 8 July 2004.

*Engineer, Research and Technology Directorate. Fellow AIAA.

is the variable-density Pridmore-Brown[23] operator,

$$\widetilde{c^2} \equiv \gamma \bar{p}/\bar{\rho}(x_2, x_3) \tag{4}$$

is the square of the mean-flow sound speed, γ is the specific heat ratio, t is the time,

$$\frac{\mathrm{D}}{\mathrm{D}t} \equiv \frac{\partial}{\partial t} + U\frac{\partial}{\partial x_1} \tag{5}$$

is the convective derivative based on U,

$$p'_e \equiv p' + [(\gamma - 1)/2]\rho v'_i v'_i \tag{6}$$

is a generalized pressure fluctuation,

$$e'_{ij} \equiv -\rho v'_i v'_j + [(\gamma - 1)/2]\delta_{ij}\rho v'^2 + \sigma'_{ij} \tag{7}$$

is the generalized stress tensor, and

$$\eta'_i \equiv -\rho v'_i h'_0 - q'_i + \sigma_{ij} v'_j \tag{8}$$

is the generalized stagnation enthalpy flux. Here,

$$v'_i \equiv v_i - \delta_{i1} U \tag{9}$$

$$h'_0 \equiv h' + \tfrac{1}{2}v'^2 \tag{10}$$

$$h' \equiv h - [\gamma/(\gamma - 1)](\bar{p}/\bar{\rho}) \tag{11}$$

are fluctuating quantities with h the enthalpy and σ'_{ij} and q'_i the fluctuating viscous stress and heat flux vector, respectively, which are believed to play a negligible direct role in the sound-generation process[21,22] and are, therefore, neglected subsequently. The fluctuating enthalpy flux η'_i will also be neglected because, as noted in the Introduction, this quantity is generally considered to be unimportant for cold jets,[2,9,10] except perhaps at small angles to the downstream axis.[12]

Then Eq. (2) can be formally solved in terms of the free-space Greens function $G(\boldsymbol{x}, t|\boldsymbol{y}, \tau)$, which satisfies (see Ref. 24)

$$LG(\boldsymbol{x}, t|\boldsymbol{y}, \tau) = \delta(\boldsymbol{x} - \boldsymbol{y})\delta(t - \tau) \tag{12}$$

and has outgoing wave behavior at infinity, to obtain the following expression

$$\overline{p^2}(\boldsymbol{x}, t_0) = \int_{-\infty}^{\infty}\iiint_V \bar{\gamma}_{ijkl}(\boldsymbol{x}|\boldsymbol{y}; \boldsymbol{\eta}, t_0 + \tau_0) R_{ijkl}(\boldsymbol{y}; \boldsymbol{\eta}, \tau_0)\,\mathrm{d}\boldsymbol{y}\,\mathrm{d}\boldsymbol{\eta}\,\mathrm{d}\tau_0 \tag{13}$$

for the pressure autocovariance[25,26] (notice that p'_e reduces to p' in the far field)

$$\overline{p^2}(\boldsymbol{x}, t_0) \equiv \frac{1}{2T}\int_{-T}^{T} p'_e(\boldsymbol{x}, t)\, p'_e(\boldsymbol{x}, t + t_0)\,\mathrm{d}t \tag{14}$$

where V denotes integration over all space, T denotes some large but finite time interval, the propagation factor $\overline{\gamma_{ij}}(\boldsymbol{x}, t|\boldsymbol{y}, \tau)$ is defined in Appendix A, and

$$R_{ijkl}(\boldsymbol{y}; \boldsymbol{\eta}, \tau_0) \equiv \frac{1}{2T}\int_{-T}^{T} \rho v'_i v'_j(\boldsymbol{y}, \tau)\rho v'_k v'_l(\boldsymbol{y} + \boldsymbol{\eta}, \tau + \tau_0)\,\mathrm{d}\tau \tag{15}$$

is the density-weighted fourth-order two-point time-delayed fluctuating velocity correlation, with the indicated arguments referring to all three terms preceding the parentheses. The details are given in Appendix A.

Lighthill[21,22] pointed out that acoustic predictions tend to be less dependent on the detailed structure of the turbulence when variations in retarded time across the correlation volume $\Delta\boldsymbol{\eta}$ can be neglected, which is a reasonable approximation in a reference frame

$$\boldsymbol{\xi} \equiv \boldsymbol{\eta} - \hat{\boldsymbol{\imath}} U_c \tau_0 \tag{16}$$

moving with the local convection velocity $U_c(\boldsymbol{y})$ of the turbulence. Ffowcs Williams[13] showed that this idea is best implemented by introducing the moving frame correlation tensor

$$R^M_{ijkl}(\boldsymbol{y}; \boldsymbol{\xi}, \tau) \equiv R_{ijkl}(\boldsymbol{y}; \boldsymbol{\xi} + \hat{\boldsymbol{\imath}} U_c \tau_0, \tau_0) \tag{17}$$

into the relevant pressure autocovariance formula [Eq. (13) in our case] to obtain

$$\overline{p^2(\boldsymbol{x}, t_0)} = \int_{-\infty}^{\infty}\iiint_V \bar{\gamma}_{ijkl}(\boldsymbol{x}|\boldsymbol{y}; \boldsymbol{\xi} + \hat{\boldsymbol{\imath}} U_c \tau_0, t_0 + \tau_0) \times R^M_{ijkl}(\boldsymbol{y}; \boldsymbol{\xi}, \tau_0)\,\mathrm{d}\boldsymbol{y}\,\mathrm{d}\boldsymbol{\xi}\,\mathrm{d}\tau_0 \tag{18}$$

Our interest is in the far-field spectrum,

$$I_\omega(\boldsymbol{x}) \equiv \frac{1}{2\pi}\int_{-\infty}^{\infty} e^{i\omega t_0}\overline{p^2}(\boldsymbol{x}, t_0)\,\mathrm{d}t_0 \tag{19}$$

which can, in principle, be calculated by taking the Fourier transform of Eq. (18) and using the convolution theorem.[24] Unfortunately, this cannot be done in practice because the Fourier transform of $R_{ijkl}(\boldsymbol{y}; \boldsymbol{\eta}, \tau_0)$ and, therefore, of $R^M_{ijkl}(\boldsymbol{y}; \boldsymbol{\xi}, \tau)$ does not exist; see p. 179 of Ref. 19. This difficulty can be overcome by replacing $R_{ijkl}(\boldsymbol{y}; \boldsymbol{\eta}, \tau_0)$ with $R_{ijkl}(\boldsymbol{y}; \boldsymbol{\eta}, \tau_0) - R_{ij}(\boldsymbol{y}; \boldsymbol{0}, 0)R_{kl}(\boldsymbol{y}; \boldsymbol{0}, 0)$, where $R_{ij}(\boldsymbol{y}; \boldsymbol{\eta}, \tau_0)$ is defined by Eq. (41) (to follow). This does not change the radiated sound because $R_{ij}(\boldsymbol{y}; \boldsymbol{0}, 0)R_{kl}(\boldsymbol{y}; \boldsymbol{0}, 0)$ is steady and, therefore, produces no sound. It then follows that

$$I_\omega(\boldsymbol{x}|\boldsymbol{y}) = 2\pi\int_{-\infty}^{\infty}\int_V \Gamma_{ij}(\boldsymbol{x}|\boldsymbol{y}; \boldsymbol{\omega})\Gamma^*_{kl}(\boldsymbol{x}|\boldsymbol{y} + \boldsymbol{\xi} + \hat{\boldsymbol{\imath}} U_c \tau_0; \boldsymbol{\omega}) e^{-i\omega\tau_0} \times R^M_{ijkl}(\boldsymbol{y}, \boldsymbol{\xi}, \tau_0)\,\mathrm{d}\boldsymbol{\xi}\,\mathrm{d}\tau_0 \tag{20}$$

where

$$\Gamma_{ij} \equiv \frac{1}{2\pi}\int_{-\infty}^{\infty} e^{i\omega(t-\tau)}\gamma_{ij}(\boldsymbol{x}|\boldsymbol{y}, t - \tau)\,\mathrm{d}(t - \tau) \tag{21}$$

is the Fourier transform of γ_{ij}. (Capital letters are used to denote Fourier transform of the corresponding lower case quantity.) We introduced $I_\omega(\boldsymbol{x}|\boldsymbol{y})$, the acoustic spectrum at $\boldsymbol{x}$ due to a unit volume of turbulence at $\boldsymbol{y}$, that is,

$$I_\omega(\boldsymbol{x}) = \int_V I_\omega(\boldsymbol{x}|\boldsymbol{y})\,\mathrm{d}\boldsymbol{y} \tag{22}$$

to simplify the formulas.[25] The relevant far-field expansion of Γ_{ij} is given in Appendix B.

The only approximation made up to this point is the neglect of the enthalpy and viscous source terms, but Eq. (20) will depend on the turbulent source correlations only through

$$\mathcal{R}_{ijkl}(\boldsymbol{y}, \tau_0) \equiv \int_V R^M_{ijkl}(\boldsymbol{y}, \boldsymbol{\xi}, \tau_0)\,\mathrm{d}\boldsymbol{\xi} \tag{23}$$

if variations in retarded time across the correlation volume are neglected, that is, if $\Gamma^*_{kl}(\boldsymbol{x}|\boldsymbol{y} + \boldsymbol{\xi} + \hat{\boldsymbol{\imath}} U_c \tau_0; \boldsymbol{\omega})$ is assumed to be constant over the correlation volume.[13] However, definition (17) implies that the integration variable in Eq. (23) can be changed back to $\boldsymbol{\eta}$, which means that

$$\mathcal{R}_{ijkl}(\boldsymbol{y}, \tau_0) = \int_V R_{ijkl}(\boldsymbol{y}, \boldsymbol{\eta}, \tau_0)\,\mathrm{d}\boldsymbol{\eta} \tag{24}$$

that is, the source correlation can be expressed in either the fixed or moving frame once the retarded time is neglected. (However, introduction of the moving frame is necessary to get the correct τ_0 dependence in Γ^*_{kl}.)

Equation (20) can now be written more simply as

$$I_\omega(\boldsymbol{x}|\boldsymbol{y}) \to (2\pi/x)^2(2\pi\omega/c_\infty)\sin\theta\,\bar{\Gamma}_{ij}(\boldsymbol{x}|\boldsymbol{y}_\perp)\bar{\Gamma}^*_{kl}(\boldsymbol{x}|\boldsymbol{y}_\perp) \times \Phi^*_{ijkl}(\boldsymbol{y}; \omega(1 - M_c\cos\theta)), \qquad \text{as} \quad x \to \infty \tag{25}$$

where

$$\Phi_{ijkl}(\boldsymbol{y},\omega) \equiv \frac{1}{2\pi}\int_{-\infty}^{\infty} e^{i\omega\tau_0}\mathcal{R}_{ijkl}(\boldsymbol{y},\tau_0)\,\mathrm{d}\tau_0 \tag{26}$$

is the spectral tensor of the source correlation and

$$M_c \equiv U_c/c_\infty \tag{27}$$

is the convective Mach number of the turbulence. This result shows that it is only necessary to model the overall spectral tensor itself and not the detailed two-point time delayed correlations of the turbulence. However, the radiated sound should still be relatively insensitive to the detailed turbulence structure even when the latter quantities are modeled (as will at least partially be done subsequently). This would not be the case if the moving frame had not been introduced before neglecting the retarded time variations.[13,25]

Our interest here is in the spectrum at 90 deg to the jet axis where $\cos\theta = 0$. Appendix B shows that

$$I_\omega(\boldsymbol{x}|\boldsymbol{y}) = \frac{(\omega/c_\infty)^4}{(4\pi x)^2}\left[\frac{x_i x_j}{x^2} - \frac{\gamma-1}{2}\delta_{ij} + \frac{i(\gamma-1)\delta_{1i}}{\omega}\frac{\partial U}{\partial y_j}\right] \times\left[\frac{x_k x_l}{x^2} - \frac{\gamma-1}{2}\delta_{kl} - \frac{i(\gamma-1)}{\omega}\delta_{1k}\frac{\partial U}{\partial y_l}\right]\Phi^*_{ijkl}(\boldsymbol{y};\omega) \quad \text{for} \quad \theta = \frac{\pi}{2} \tag{28}$$

when $\widetilde{c_0^2} = c_\infty^2 =$ constant, that is, in the isothermal case.

III. Quasi-Normal and Axisymmetric Turbulence Approximations

To proceed further, we need to know something about the source spectral tensor Φ_{ijkl}. The usual approach[14,15,18] is to begin by assuming that the turbulence is quasi normal[12,19] to obtain some relations between its components. It then follows that

$$R_{ijkl}(y;\boldsymbol{\eta},\tau_0) = R_{ik}(y;\boldsymbol{\eta},\tau_0)R_{jl}(y;\boldsymbol{\eta},\tau_0) + R_{il}(y;\boldsymbol{\eta},\tau_0)R_{jk}(y;\boldsymbol{\eta},\tau_0) \tag{29}$$

where

$$R_{ij}(\boldsymbol{y};\boldsymbol{\eta},\tau_0) \equiv \frac{1}{2T}\int_{-T}^{T}\sqrt{\rho}\,v_i'(\boldsymbol{y},\tau_0)\sqrt{\rho}\,v_j'(\boldsymbol{y}+\boldsymbol{\eta},\tau+\tau_0)\,\mathrm{d}\tau \tag{30}$$

is the second-order correlation. [See comments preceding Eq. (20) and following Eq. (15).] To further reduce the number of independent components, it is usual to assume some kinematically possible symmetric form for the second-order correlations. Early studies[27] assumed the turbulence to be isotropic, but that turns out to be incompatible with the Harper-Bourne[20] measurements, to be introduced. The simplest assumption compatible with his results is the one introduced in Refs. 14 and 15, namely, that the turbulence is axisymmetric, which implies that[19]

$$R_{ij}(\boldsymbol{y};\boldsymbol{\eta},\tau_0) = A_0\eta_i\eta_j + B_0\delta_{ij} + C_0\delta_{1i}\delta_{1j} + D_0(\delta_{1j}\eta_j + \delta_{1j}\eta_i) \tag{31}$$

where A_0, B_0, C_0, and D_0 are functions of $\boldsymbol{y}$, τ_0, and $\eta_\perp \equiv \sqrt{(\eta_2^3+\eta_3^2)}$; A_0, B_0, and C_0 are even functions $\eta_\perp$; and D_0 is an odd function of this quantity. This model is chosen because it is the most general of those whose mathematical properties have been studied in the literature and because it is consistent with the observation that the crossflow velocity components tend to be much more similar to one another than to the streamwise component, even for nonaxisymmetric flows. Inserting Eq. (31) into Eq. (29) and inserting the result into Eq. (25) via Eqs. (23) and (26) yields (after a straightforward but tedious calculation that follows along the lines of the one in Appendix A of Ref. 14)

$$I_\omega(\boldsymbol{x}|\boldsymbol{y})(4\pi x)^2 = 2(\omega/c_\infty)^4\left\{\Phi_1 - (\gamma-1)\Phi_2 + [(\gamma-1)/2]^2\Phi_3\right\} + [(\gamma-1)(\omega/c_\infty)|\nabla M||]^2\Phi_4 \tag{32}$$

where

$$\Phi_1 \equiv \frac{1}{2\pi}\int_{-\infty}^{\infty} e^{-i\omega\tau_0}\int_V R_{22}^2(\boldsymbol{y},\boldsymbol{\eta},\tau_0)\,\mathrm{d}\boldsymbol{\eta}\,\mathrm{d}\tau_0 \tag{33a}$$

$$\Phi_2 \equiv \frac{1}{2\pi}\int_{-\infty}^{\infty} e^{-i\omega\tau_0}\int_V \left(R_{23}^2 + R_{12}^2 + R_{22}^2\right)\mathrm{d}\boldsymbol{\eta}\,\mathrm{d}\tau_0 \tag{33b}$$

$$\Phi_3 \equiv \frac{1}{2\pi}\int_{-\infty}^{\infty} e^{-i\omega\tau_0}\int_V \left(4R_{12}^2 + 2R_{23}^2 + R_{11}^2 + 2R_{22}^2\right)\mathrm{d}\boldsymbol{\eta}\,\mathrm{d}\tau_0 \tag{33c}$$

$$\Phi_4 \equiv \frac{1}{2\pi}\int_{-\infty}^{\infty} e^{-i\omega\tau_0}\int_V \left(R_{12}^2 + R_{11}R_{22}\right)\mathrm{d}\boldsymbol{\eta}\,\mathrm{d}\tau_0 \tag{33d}$$

are seemingly independent spectral functions. However, the coefficients A_0, B_0, C_0, and D_0 in Eq. (31) are not all independent, and when compressibility effects are neglected, that is, when ρ is treated as a constant, these turbulence correlations can be expressed in terms of two independent scalar functions of $\boldsymbol{y}$, τ_0, $\eta_\perp$, and η_1, which we denote by a and b, both of which are even functions of the latter variable.[16,17,28] The resulting expressions for the two-point correlations are given in Appendix C, where they are used to express the integrals over V in Eqs. (33) in terms of a and b. Equations (C1–C4) suggest that these latter quantities will scale like

$$b = \widetilde{\rho u_1^2}B(\tilde{\eta}_\perp,\tilde{\eta}_1)L_\perp^2\big/2 \tag{34}$$

$$g \equiv a - b_{\eta_1\eta_1} = \widetilde{\rho u_2^2}D(\tilde{\eta}_\perp,\tilde{\eta}_1) \tag{35}$$

where

$$\tilde{\eta}_1 \equiv \eta_1/L_1 \tag{36}$$

$$\tilde{\eta}_\perp \equiv \eta_\perp/L_\perp \tag{37}$$

L_1 and $L_\perp$ denote characteristic streamwise and transverse length scales of the turbulence, B and D are $\mathcal{O}(1)$ functions of the indicated arguments,

$$\widetilde{\rho u_1^2} \equiv R_{11}(\boldsymbol{0},0) \tag{38}$$

$$\widetilde{\rho u_2^2} \equiv R_{22}(\boldsymbol{0},0) \tag{39}$$

Turbulence measurements suggest that

$$\varepsilon \equiv L_\perp/4L_1 \tag{40}$$

ought to be small. In fact, Harper-Bourne's[20] measurements (to be discussed) suggest that $\varepsilon \simeq 2.7\times10^{-2}$. Scalings (34–40) are inserted into Eqs. (C5–C9) of Appendix C, where it is shown that

$$\frac{(4/3)\Phi_1}{2\pi L_1L_\perp^2\left(\widetilde{\rho u_1^2}\right)^2} = \frac{\Phi_2}{2\pi L_1L_\perp^2\left(\widetilde{\rho u_1^2}\right)^2} \tag{41a}$$

$$\frac{(4/3)\Phi_1}{2\pi L_1L_\perp^2\left(\widetilde{\rho u_1^2}\right)^2} = r^2\int_{-\infty}^{\infty} e^{-i\omega\tau_0}\int_{-\infty}^{\infty}\int_0^{\infty}\left(\tilde{\eta}_\perp\frac{\partial D}{\partial\tilde{\eta}_\perp}\right)^2 \times\tilde{\eta}_\perp\,\mathrm{d}\tilde{\eta}_\perp\,\mathrm{d}\tilde{\eta}_1\,\mathrm{d}\tau_0 \tag{41b}$$

$$\frac{\Phi_3}{2\pi L_1L_\perp^2\left(\widetilde{\rho u_1^2}\right)^2} = \int_{-\infty}^{\infty} e^{-i\omega\tau_0}\int_{-\infty}^{\infty}\int_0^{\infty}\left[\frac{\bar{B}^2}{8} + 2r^2\left(\tilde{\eta}_\perp\frac{\partial D}{\partial\tilde{\eta}_\perp}\right)^2\right] \times\tilde{\eta}_\perp\,\mathrm{d}\tilde{\eta}_\perp\,\mathrm{d}\tilde{\eta}_1\,\mathrm{d}\tau_0 \tag{41c}$$

$$\frac{\Phi_4}{2\pi L_1L_\perp^2\left(\widetilde{\rho u_1^2}\right)^2} = \frac{r}{2}\int_{-\infty}^{\infty} e^{-i\omega\tau_0}\int_{-\infty}^{\infty}\int_0^{\infty}\bar{B}\left(\frac{\partial}{\partial\tilde{\eta}_\perp}\tilde{\eta}_\perp^2 D\right) \times\mathrm{d}\tilde{\eta}_\perp\,\mathrm{d}\tilde{\eta}_1\,\mathrm{d}\tau_0 \tag{41d}$$

when $\mathcal{O}(\varepsilon^2)$ terms are neglected. The ratio r is defined by

$$r \equiv \widetilde{\rho u_2^2} \Big/ \widetilde{\rho u_1^2} \tag{42}$$

Lacking any specific data to the contrary, it seems reasonable to suppose that

$$\Phi_0 \equiv \frac{1}{\pi}\int_{-\infty}^{\infty} e^{-i\omega\tau_0}\int_V R_{11}^2(\boldsymbol{y},\boldsymbol{\eta},\tau_0)\,\mathrm{d}\boldsymbol{\eta}\,\mathrm{d}\tau_0$$

$$= \frac{1}{(\Gamma r)^2}\frac{1}{\pi}\int_{-\infty}^{\infty} e^{-i\omega\tau_0}\int_V R_{22}^2(\boldsymbol{y},\boldsymbol{\eta},\tau_0)\,\mathrm{d}\boldsymbol{\eta}\,\mathrm{d}\tau_0 \tag{43}$$

with $r=$ constant, that is, independent of ω. Equation (32) then becomes

$$I_\omega(\boldsymbol{x}|\boldsymbol{y})(2\pi x c_\infty)^2 = c_0^2\Phi_0(\boldsymbol{y},\omega)(\omega/c_\infty)^2\left[\omega^2+(U_c\kappa)^2\right] \tag{44}$$

where

$$2C_0^2 \equiv \tfrac{2}{3}(\Gamma r)^2\left\{\tfrac{3}{4}-(\gamma-1)+2[(\gamma-1)/2]^2\right\}+\tfrac{1}{2}[(\gamma-1)/2]^2 \tag{45}$$

is a constant and

$$\kappa \equiv \left(\frac{\gamma-1}{2}\right)\frac{|\nabla U|}{U_c C_0}$$

$$\times\sqrt{\frac{2r\int_{-\infty}^{\infty}e^{-i\omega\tau_0}\int_{-\infty}^{\infty}\int_0^{\infty}\bar{B}\left[(\partial/\partial\tilde{\eta}_\perp)\tilde{\eta}_\perp^2 D\right]\mathrm{d}\tilde{\eta}_\perp\,\mathrm{d}\tilde{\eta}_1\,\mathrm{d}\tau_0}{\int_{-\infty}^{\infty}e^{-i\omega\tau_0}\int_{-\infty}^{\infty}\int_0^{\infty}\bar{B}^2\tilde{\eta}_\perp\,\mathrm{d}\tilde{\eta}_\perp\,\mathrm{d}\tilde{\eta}_1\,\mathrm{d}\tau_0}} \tag{46}$$

IV. Harper-Bourne Spectrum

The results cannot be made more explicit without inputting more specific information about the turbulence structure. This is accomplished with the aid of some recent measurements[20] of the two-point fourth-order streamwise velocity correlation spectra along the centerline of the mixing layer in a low Mach number jet, which would most closely correspond to

$$H_0(\boldsymbol{y},\boldsymbol{\eta},\omega) \equiv \frac{1}{\pi}\int_{-\infty}^{\infty} e^{-i\omega\tau_0}R_{11}^2(\boldsymbol{y},\boldsymbol{\eta},\tau_0)\,\mathrm{d}\tau_0 \tag{47}$$

with the quasi-normal approximation that is being used in the present analysis.

Harper-Bourne[20] divided H_0 into the three components [Ref. 20, Eqs. (2.5) and (2.7), p. 2],

$$H_0 = H_0(\boldsymbol{y},\boldsymbol{0},\omega)R(\boldsymbol{y},\eta_1/l_1,\eta_\perp/l_\perp,\omega)e^{i\omega\tau_p} \tag{48}$$

where l_1 and $l_\perp$ are the spectral streamwise and transverse length scales (not necessarily the same as the time-domain length scales L_1 and $L_\perp$ introduced earlier) and

$$\tau_p \simeq \eta_1/U_c \tag{49}$$

No assumption is made about the decomposition of the correlations into products of their space and time components with this approach.

The first factor can be evaluated from his measurements of $R_{1111}(\boldsymbol{y},\boldsymbol{0},\tau_0)$, which are well represented by the exponential $e^{-\lambda|\tau_0|}$, which in turn implies that

$$H_0(\boldsymbol{y},\boldsymbol{0},\omega) = \frac{\lambda\widetilde{\rho^2 u_1^4}}{\pi(\lambda^2+\omega^2)} \tag{50}$$

Inserting these into Eq. (43) and using the result in Eq. (44) shows that

$$I_\omega(\boldsymbol{x}|\boldsymbol{y}) = C_0^2\frac{\lambda\widetilde{\rho u_1^4}\left[\omega^2+(U_c\kappa)^2\right]}{x^2c_\infty^4(\lambda^2+\omega^2)\omega}2U_c^3\bar{l}_1\bar{l}_\perp^2\bar{R}(\boldsymbol{y},\bar{l}_1) \tag{51}$$

where

$$\bar{R}(\boldsymbol{y},\bar{l}_1) \equiv 2\pi\int_{-\infty}^{\infty}\int_0^{\infty}R(\boldsymbol{y},\bar{\eta}_1,\bar{\eta}_\perp)\exp(-2\pi i\bar{\eta}_1\bar{l}_1)\,\mathrm{d}\bar{\eta}_1\bar{\eta}_\perp\,\mathrm{d}\bar{\eta}_\perp \tag{52}$$

and $\bar{l}_1$ and $\bar{l}_\perp$ are defined by

$$\bar{l}_1 \equiv \omega l_1/2\pi U_c \tag{53}$$

$$\bar{l}_\perp \equiv \omega l_\perp/2\pi U_c \tag{54}$$

Harper-Bourne's measurements seem to indicate that $R(\boldsymbol{y},\bar{\eta}_1,0)$ behaves like $e^{-|\bar{\eta}_1|}$, which, as pointed out by Khavaran et al.,[29] is inconsistent with Hinze's[28] parabolic vertex requirement. We, therefore, apply a Gaussian filter to Harper-Bourne's measured value of R, which we denote by R_m, to obtain

$$R(\boldsymbol{y},\bar{\eta}_1,\bar{\eta}_\perp) = \frac{\int_{-\infty}^{\infty}\exp\left\{-[(\bar{\eta}_1-\hat{\eta}_1)/2\beta]^2\right\}R_m(\boldsymbol{y},\hat{\eta}_1,\bar{\eta}_\perp)\,\mathrm{d}\hat{\eta}_1}{\sqrt{\pi}\exp(\beta/l_1)^2\operatorname{erfc}(\beta/l_1)} \tag{55}$$

which smoothes out the cusp at $\bar{\eta}_1=0$, but otherwise behaves similarly to R_m. (Note the data scatter around $\eta_1=0$ in Harper-Bourne's Fig. 14a.) The error function factor, $\exp(\beta/l_1)^2\operatorname{erfc}(\beta/l_1)$, has been inserted in the denominator to ensure that R still satisfies the normalization condition, $R(\boldsymbol{y},0,0)=1$, when $R_m(\boldsymbol{y},\bar{\eta}_1,0)=e^{-|\bar{\eta}_1|}$. In fact, it is easy to show more generally that

$$R(\boldsymbol{y},\bar{\eta}_1,0) = \frac{e^{-\bar{\eta}_1}\operatorname{erfc}(\beta/l_1-\bar{\eta}_1 l_1/2\beta)+e^{\bar{\eta}_1}\operatorname{erfc}(\beta/l_1+\bar{\eta}_1 l_1/2\beta)}{2\operatorname{erfc}(\beta/l_1)} \tag{56}$$

which behaves like $e^{-|\bar{\eta}_1|}$ for large η_1 but has continuous slope at $\eta_1=0$.

Inserting Eq. (55) into Eq. (52), using the convolution theorem,[24] and inserting the result into Eq. (51) yields

$$I_\omega(\boldsymbol{x}|\boldsymbol{y}) = C_0^2\frac{\lambda\widetilde{\rho u_1^4}\exp\left[-(\beta\omega/U_c)^2\right]\left[\omega^2+(U_c\kappa)^2\right]2U_c^3\bar{l}_1\bar{l}_\perp^2\bar{R}_m(\boldsymbol{y},\bar{l}_1)}{x^2c_\infty^4\exp(\beta/l_1)^2\operatorname{erfc}(\beta/l_1)(\lambda^2+\omega^2)\omega} \tag{57}$$

where

$$\bar{R}_m(\boldsymbol{y},\bar{l}_1) \equiv 2\pi\int_{-\infty}^{\infty}\int_0^{\infty}R_m(\boldsymbol{y},\bar{\eta}_1,\bar{\eta}_\perp)\exp(-2\pi i\bar{\eta}_1\bar{l}_1)\,\mathrm{d}\bar{\eta}_1\bar{\eta}_\perp\,\mathrm{d}\bar{\eta}_\perp \tag{58}$$

which reduces to Eq. (51) when $\beta=0$.

V. Comparison with Tam and Auriault Result

The form

$$R_m = e^{-\bar{\eta}_\perp^2}e^{-|\bar{\eta}_1|} \tag{59}$$

agrees fairly well with Harper-Bourne's measurements[20] when $\eta_1=0$ and $\eta_\perp\neq 0$ and also when $\eta_\perp=0$ and $\eta_1\neq 0$. Inserting this into Eq. (58), integrating over $\boldsymbol{\eta}$, and inserting the result into Eq. (57) shows that

$$I_\omega(\boldsymbol{x}|\boldsymbol{y}) = C_0^2\frac{\lambda\widetilde{\rho u_1^4}\exp\left[-(\beta\omega/U_c)^2\right]2U_c^5\bar{l}_1\bar{l}_\perp^2\kappa^2}{x^2c_\infty^4\exp(\beta/l_1)^2\operatorname{erfc}(\beta/l_1)(\lambda^2+\omega^2)\omega}$$

$$\times\left[\frac{1+(\omega/U_c\kappa)^2}{1+(2\pi\bar{l}_1)^2}\right] \tag{60}$$

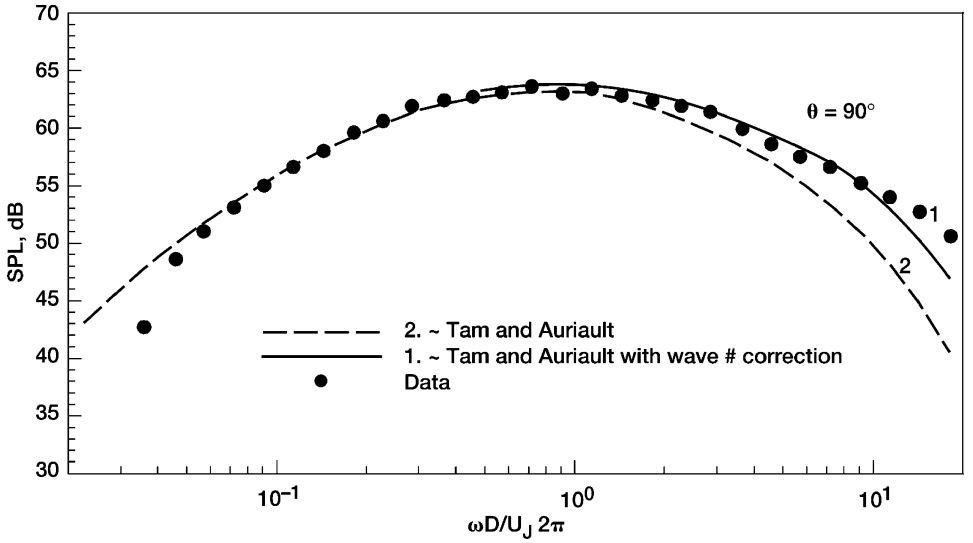

Fig. 1 Mach 0.5 cold jet 90-deg spectal predictions (based on Ref. 29).

Form (59) is consistent with the assumption that $B/2 = G = \bar{a}(\bar{\eta}_1, \tau_0)\exp(-\bar{\eta}_\perp^2/2)$ when l_1 and $l_\perp$ are taken to be constants, that is, independent of ω, which then implies that the ratio of integrals in Eq. (46) is equal to $\frac{1}{2}$ and that $\Gamma^2 = 3$ in Eq. (43). It follows that for $r = \frac{1}{2}$, $\gamma = 1.4$, and $U_c = 0.65\,U_J$,

$$\kappa \approx |\nabla U|/U_J 2 \approx 1/2 l_s D_J \tag{61}$$

where $l_s \approx 0.345$ is the characteristic length scale of the mean velocity divided by the jet diameter D_J. Harper-Bourne's measurements show that $l_\perp$ and 1_1 are relatively constant and that the latter can be approximated by $l_1 \approx 0.691 D_J$ at sufficiently low frequencies. Therefore, it follows that the square bracket in Eq. (60) is approximately equal to unity, which means that the resulting 90-deg acoustic spectrum should be of the form

$$I_\omega(\boldsymbol{x}|\boldsymbol{y}) \propto \frac{\exp\left[-(\beta\omega/U_c)^2\right]\omega^2}{(\omega^2 + \lambda^2)} \tag{62}$$

which is the same as the spectral form proposed by Tam and Auriault,[5] who take $\beta l_1/U_c = (c_l/2\varepsilon)(k^{3/2}/\bar{u})$ and $\lambda = \varepsilon/c_\tau k$ [Eq. (53) of Ref. 4], where c_l and c_τ adjustable constants and k and ε (not to be confused with the ε in Eq. (40)] are determined from a k–ε RANS calculation. Notice that in this result I_ω behaves like ω^2 as $\omega \to 0$ and converges like $\exp[-(\beta\omega/U_c)^2]$ as $\omega \to \infty$.

However, Harper-Bourne demonstrates that the separable form (59) does not work at oblique separations where η_1 and $\eta_\perp$ are both nonzero and, more important, his Fig. 13 shows that l_1 and $l_\perp$ are only constant at relatively low frequencies and that it is the scaled length scales $\bar{l}_i$ and $\bar{l}_\perp$ that become constant when $\omega \to \infty$. Therefore, it follows from Eq. (57) and the asymptotic behavior of the error function (Ref. 30, p. 298, #7.1.23) that $I_\omega(\boldsymbol{x}|\boldsymbol{y})$ converges like $\exp[-(\beta\omega/U_c)^2]$ when $\kappa \approx$ const and $\omega \to \infty$, that is, it has the same high-frequency behavior as the Tam and Auriault result (62). The general formula (57), therefore, coincides with that result at both high and low to moderately low frequencies, even with frequency-dependent length scales.

The two results differ at intermediate to moderately high frequencies by the factor

$$\frac{\exp\left(\beta/l_1^{(0)}\right)^2 \operatorname{erfc}\left(\beta/l_1^{(0)}\right)}{\exp(\beta/l_1)^2 \operatorname{erfc}(\beta/l_1)} \left[\frac{1 + (\omega/U_c\kappa)^2}{1 + (2\pi\bar{l}_1)^2}\right] \left(\frac{l_1}{l_1^{(0)}}\right)^2 \left(\frac{l_\perp}{l_\perp^{(0)}}\right) \tag{63}$$

(where $l_1^{(0)} = 0.691 D$ and $l_\perp^{(0)}$ are the initial constant values of l_1 and $l_\perp$), which is no longer equal to unity at these frequencies but becomes constant as $\omega \to \infty$. On the other hand, Khavaran et al.[29] point out that the Tam and Auriault[5] data comparisons do not account for atmospheric attenuation. Figure 1 (taken, in part, from Ref. 29) shows that the latter comparisons (curve 2) underpredict the high-frequency portion of the spectrum for a Mach number 0.5 cold jet when atmospheric absorption effects are included. However, multiplying the Tam and Auriault result by the correction factor (63) (with l_1 and $l_\perp$ given by the formulas in Harper-Bourne's Fig. 13), which is hopefully relatively independent of the choice of observation point, leads to curve 1, which is in much better agreement with the data. It would, of course, be better to sum the actual formula (57) over the jet with appropriate local values for the parameters, but because the measurements are all at a single location, this does not seem to be warranted at the present time.

Harper-Bourne obtains the best fit to his data with the nonseparable form

$$R_m = \exp\left(-\sqrt{\bar{\eta}_1^2 + \bar{\eta}_\perp^4}\right) \tag{64}$$

which can be inserted into Eq. (57) via Eq. (58) to obtain

$$I_\omega(\boldsymbol{x}|\boldsymbol{y}) = C_0^2 \frac{\lambda\rho\widetilde{u_1^4}\exp\left[-(\beta\omega/U_c)^2\right]\left[\omega^2 + (U_c\kappa)^2\right]\pi U_c^3 \overline{l_1 l_\perp^2}}{x^2 c_\infty^4 \left[\exp(\beta/l_1)^2 \operatorname{erfc}(\beta/l_1)\right](\lambda^2 + \omega^2)\omega\left[1 + (2\pi\bar{l}_1)^2\right]^{\frac{3}{2}}} \tag{65}$$

which has the same high- and low-frequency behavior as Eq. (60) but is slightly different from it at intermediate frequencies. More in-depth data comparisons may be needed to determine whether this result will provide a better representation of the data.

VI. Discussion

As noted in the Introduction, Morris and Farassat[4] argue that, for the same mean-flow calculation, the Tam and Aurialt result (62) yields a better prediction of the 90-deg acoustic spectrum than methods based on the usual acoustic-analogy approximations. They also show that this type of spectrum can be obtained within the acoustic analogy frame work if the usual source modeling is applied to $(\mathrm{D}^2/\mathrm{D}\tau_0^2)R_{ijkl}$ rather than to R_{ijkl} as was done earlier. However, this would imply that the R_{ijkl} spectrum becomes infinite like ω^2 as $\omega \to 0$, which is certainly not consistent with experimental results. The conventional acoustic-analogy approach leads to a multiplicative factor of ω^4 in the spectrum[25] [rather than the ω^2 factor in Eq. (62)] due to the quadrapole nature of the source. The ω^2 factor is more characteristic of a dipole source at low frequencies. In the present approach, the energy equation introduces the dipole type source term $-(\partial U/\partial x_i)(\gamma - 1)(\mathrm{D}^2/\mathrm{D}t^2)e'_{1i}$ in the acoustic-analogy Eq. (2), which combines with the quadrupole source and a portion

of the physically realizable spectral function, Eq. (48), that arises from the nonseparable nature of the source to produce the correct spectral form.

VII. Conclusions

Whereas the 90-deg spectrum is useful from a diagnostics point of view, the maximum acoustic intensity occurs at relatively small angles to the downstream axis for most (if not all) high-speed air jets. The predictions of the present model would differ from the Tam and Auriault[5] results at these angles or, for that matter, from any modification of the conventional acoustic analogy.

Appendix A: Pressure Autocovariance

The formal Green's function solution to Eq. (2) can be written as

$$p'_e(\boldsymbol{x},t)=\int_V\int_{-\infty}^{\infty}\rho v'_i v'_j\gamma_{ij}(\boldsymbol{x},t|\boldsymbol{y},\tau)\,\mathrm{d}\boldsymbol{y}\,\mathrm{d}\tau \tag{A1}$$

where $\rho v'_i v'_j$ is evaluated at $\boldsymbol{y},\tau$,

$$\gamma_{ij}(\boldsymbol{x},t|\boldsymbol{y},\tau)\equiv\left[\left(\delta_{in}\delta_{jm}-\frac{\gamma-1}{2}\delta_{ij}\delta_{nm}\right)\left(\frac{\partial}{\partial y_m}\widetilde{c^2}\frac{\partial}{\partial y_n}\frac{\mathrm{D}}{\mathrm{D}\tau}+2\frac{\partial}{\partial y_m}\widetilde{c^2}\frac{\partial U}{\partial y_n}\frac{\partial}{\partial y_1}\right)+\delta_{1i}(\gamma-1)\frac{\partial U}{\partial y_j}\frac{\mathrm{D}^2}{\mathrm{D}\tau^2}\right]G(\boldsymbol{x},t|\boldsymbol{y},\tau) \tag{A2}$$

where all of the terms in square brackets are part of the differential operator and we have integrated by parts to transfer the derivatives from the source term to G. Inserting this into Eq. (14), changing integration variables to $t_1\equiv t-\tau_2$ and $\tau_1\equiv\tau_2-\tau$, and introducing Eq. (15) yields

$$\begin{aligned}\overline{p^2}&\equiv\frac{1}{2T}\int_{-T}^{T}\iiint_{-\infty}^{\infty}\iint_V\gamma_{ij}(\boldsymbol{x}|\boldsymbol{y},t+t_0-\tau)\gamma_{kl}(\boldsymbol{x}|\boldsymbol{y},t-\tau_2)\\&\quad\times\rho v'_i v'_j(\boldsymbol{y},\tau)\rho v'_k v'_l(\boldsymbol{y}_1,\tau_2)\,\mathrm{d}\boldsymbol{y}\,\mathrm{d}\boldsymbol{y}_1\,\mathrm{d}\tau\,\mathrm{d}\tau_2\,\mathrm{d}t\\&=\iiint_{-\infty}^{\infty}\iint_V\gamma_{ij}(\boldsymbol{x}|\boldsymbol{y},t_1+t_0+\tau_1)\gamma_{kl}(\boldsymbol{x}|\boldsymbol{y}_1,t_1)\\&\quad\times R_{ijkl}(\boldsymbol{y};\boldsymbol{y}_1-\boldsymbol{y},\tau_1)\,\mathrm{d}\boldsymbol{y}\,\mathrm{d}\boldsymbol{y}_1\,\mathrm{d}t_1\,\mathrm{d}\tau_1\end{aligned} \tag{A3}$$

which on introduction of the separation vector

$$\boldsymbol{\eta}\equiv\boldsymbol{y}_1-\boldsymbol{y} \tag{A4}$$

can be written more compactly as Eq. (13) with

$$\bar{\gamma}_{ijkl}(\boldsymbol{x}|\boldsymbol{y};\boldsymbol{\eta},t_0+\tau_0)\equiv\int_{-\infty}^{\infty}\gamma_{ij}(\boldsymbol{x},\boldsymbol{y},t_1+t_0+\tau_0)\gamma_{kl}(\boldsymbol{x}|\boldsymbol{y}+\boldsymbol{\eta},t_1)\,\mathrm{d}t_1 \tag{A5}$$

The quantities $\boldsymbol{y}_1$, t_1, and τ_1 are dummy integration variables and we are using the fact that G and, therefore, γ_{ij} depend on t and τ only in the combination $t-\tau$.

Appendix B: Far-Field Expansion and Neglect of Retarded Time

Taking Fourier transforms of Eq. (12) with respect to (x_1-y_1) and $(t-\tau)$ shows (because G can depend on these quantities only in these combinations) that

$$\widetilde{\mathcal{L}}_k\bar{G}_0=\frac{\delta(\boldsymbol{x}_\perp-\boldsymbol{y}_\perp)}{(2\pi)^2} \tag{B1}$$

where

$$\widetilde{\mathcal{L}}_k\equiv\frac{\partial}{\partial x_j}\frac{\widetilde{c_0^2}}{(kU-\omega)^2}\frac{\partial}{\partial x_j}+1-\frac{k^2\widetilde{c_0^2}}{(kU-\omega)^2},\qquad j=2,3 \tag{B2}$$

is the reduced Rayleigh operator and

$$\overline{G_0}(\boldsymbol{x}_\perp|\boldsymbol{y}_\perp;k,\omega)\equiv-i\frac{[\omega-U(\boldsymbol{y}_\perp)k]^3}{(2\pi)^2}\iint\exp\{-i[k(x_1-y_1)-\omega(t-\tau)]\}G(\boldsymbol{x},t|\boldsymbol{y},\tau)\,\mathrm{d}(t-\tau)\,\mathrm{d}(x_1-y_1) \tag{B3}$$

where $\boldsymbol{x}_\perp$ and $\boldsymbol{y}_\perp$ have the obvious meaning. Inserting this into Eqs. (21) and (A2) shows (after some rearrangement) that

$$\Gamma_{ij}=-\left(\delta_{in}\delta_{jm}-\frac{\gamma-1}{2}\delta_{ij}\delta_{nm}\right)\frac{\partial}{\partial y_m}\widetilde{c^2}\int_{-\infty}^{\infty}\frac{1}{[\omega-kU(\boldsymbol{y}_\perp)]^2}\frac{\partial}{\partial y_n}\times e^{ik(x_1-y_1)}\overline{G_0}\,\mathrm{d}k-i\delta_{1i}(\gamma-1)\frac{\partial U}{\partial y_j}\int_{-\infty}^{\infty}\frac{e^{ik(x_1-y_1)}\overline{G_0}}{[\omega-kU(\boldsymbol{y}_\perp)]}\mathrm{d}k \tag{B4}$$

This result is much simpler in the far field where $U(\boldsymbol{x}_\perp)\to 0$, $\widetilde{c_0^2}\to c_\infty^2=\text{const}$, and

$$\overline{G_0}\to\exp\left[-x_\perp\sqrt{k^2-(\omega/c_\infty)^2}\,\widetilde{\mathcal{G}}_0(\varphi,k,\omega|\boldsymbol{y}_\perp)\Big/\sqrt{x_\perp}\right]\qquad\text{as}\quad x_\perp\to\infty \tag{B5}$$

Here, $x_\perp\equiv|\boldsymbol{x}_\perp|$ and $\varphi\equiv\tan^{-1}(x_2/x_3)$ denotes the circumferential angle. Inserting this into Eq. (B4) and using stationary phase to evaluate the integrals now shows that

$$\begin{aligned}\Gamma_{ij}&\to-\frac{\exp[i\omega(x-y_1\cos\theta)/c_\infty]}{x}\sqrt{\frac{2\pi i\omega\sin\theta}{c_\infty}}\bar{\Gamma}_{ij}(\boldsymbol{x}|\boldsymbol{y}_\perp)\\&\equiv-\frac{\exp(i\omega x/c_\infty)}{x}\sqrt{\frac{2\pi i\omega\sin\theta}{c_\infty}}\left[\left(\delta_{in}\delta_{jm}-\frac{\gamma-1}{2}\delta_{ij}\delta_{nm}\right)\times\frac{\partial}{\partial y_m}\frac{\widetilde{c^2}/\omega^2}{[M(\boldsymbol{y}_\perp)\cos\theta-1]^2}\frac{\partial}{\partial y_n}-\frac{i\delta_{1i}(\gamma-1)}{\omega}\frac{\partial U}{\partial y_j}\times\frac{1}{[M(\boldsymbol{y}_\perp)\cos\theta-1]}\right]\exp\left(-\frac{i\omega y_1\cos\theta}{c_\infty}\right)\\&\quad\times\widetilde{\mathcal{G}}_0\left(\varphi,\frac{\omega}{c_\infty}\cos\theta,\omega|\boldsymbol{y}_\perp\right),\qquad\text{as}\quad x\to\infty\end{aligned} \tag{B6}$$

where $x\equiv|\boldsymbol{x}|$ is the radial coordinate, $\theta=\arcsin(x_\perp/x)$ is the polar angle of the observation point, and

$$M\equiv U(\boldsymbol{y}_\perp)/c_\infty \tag{B7}$$

is the acoustic Mach number at the source point.

Because Eq. (B2) reduces to Helmholtz's equation when $k=0$, $\overline{G_0}(\boldsymbol{x}_\perp|\boldsymbol{y}_\perp;0,\omega)$ is given by (Ref. 24, p. 811)

$$\begin{aligned}\overline{G_0}&=-\frac{i}{2(2\pi)^2}\left(\frac{\omega}{c_\infty}\right)H_0^{(1)}\left(\frac{\omega}{c_\infty}|\boldsymbol{x}_\perp-\boldsymbol{y}_\perp|\right)\\&\to-\frac{1}{2(2\pi)^3}\left(\frac{\omega}{c_\infty}\right)^2\sqrt{\frac{2\pi}{(\omega/c_\infty)x_\perp}}\\&\quad\times\exp\left[i\left(\frac{\omega}{c_\infty}|\boldsymbol{x}_\perp-\boldsymbol{y}_\perp|+\frac{\pi}{4}\right)\right],\qquad\text{as}\quad x_\perp\to\infty\end{aligned} \tag{B8}$$

when $\cos\theta=0$ and $\widetilde{c_0^2}=c_\infty^2=\text{const}$. It follows from Eqs. (B5), (B6), (23), (24), and (26) that

$$\widetilde{\mathcal{G}}_0(\varphi,0,\omega|\boldsymbol{y}_\perp)=-\frac{\exp(i\pi/4)}{2(2\pi)^3}\left(\frac{\omega}{c_\infty}\right)^2\sqrt{\frac{2\pi c_\infty}{\omega}}\exp\left(-\frac{i\omega\boldsymbol{x}_\perp\cdot\boldsymbol{y}_\perp}{c_\infty x_\perp}\right) \tag{B9}$$

and, therefore, that Eq. (25) holds.

Appendix C: Reduction of Correlation Coefficients

It is shown in Refs. 14, 16, and 17 that

$$R_{22} = a + \frac{\eta_3^2}{\eta_\perp}\frac{\partial a}{\partial \eta_\perp} - \frac{\partial^2 b}{\partial \eta_1^2} \tag{C1}$$

$$R_{23} = -\frac{\eta_2 \eta_3}{\eta_\perp}\frac{\partial a}{\partial \eta_\perp} \tag{C2}$$

$$R_{12} = \frac{\eta_2}{\eta_\perp}\frac{\partial^2 b}{\partial \eta_\perp \partial \eta_1} \tag{C3}$$

$$R_{11} = -\frac{1}{\eta_\perp}\frac{\partial}{\partial \eta_\perp}\eta_\perp \frac{\partial b}{\partial \eta_\perp} \tag{C4}$$

so that integration with respect to the circumferential coordinate shows that

$$\frac{1}{2\pi}\int_V R_{22}^2 \,\mathrm{d}\boldsymbol{\eta} = \int_{-\infty}^{\infty}\int_0^{\infty}\left[\frac{3}{8}\left(\eta_\perp \frac{\partial a}{\partial \eta_\perp}\right)^2 + \left(\frac{\partial^2 b}{\partial \eta_1^2}\right)^2 - \left(\frac{\partial^2 b}{\partial \eta_1^2}\right)\frac{1}{\eta_\perp}\frac{\partial}{\partial \eta_\perp}\left(\eta_\perp^2 a\right)\right]\eta_\perp \,\mathrm{d}\eta_\perp \,\mathrm{d}\eta_1 \tag{C5}$$

$$\frac{1}{2\pi}\int_V R_{23}^2 \,\mathrm{d}\boldsymbol{\eta} = \frac{1}{8}\int_{-\infty}^{\infty}\int_0^{\infty}\left(\frac{\partial a}{\partial \eta_\perp}\right)^2 \eta_\perp^3 \,\mathrm{d}\eta_\perp \,\mathrm{d}\eta_1 \tag{C6}$$

$$\frac{1}{2\pi}\int_V R_{12}^2 \,\mathrm{d}\boldsymbol{\eta} = \frac{3}{8}\int_{-\infty}^{\infty}\int_0^{\infty}\left(\frac{\partial^2 b}{\partial \eta_1 \partial \eta_\perp}\right)^2 \eta_\perp \,\mathrm{d}\eta_\perp \,\mathrm{d}\eta_1 \tag{C7}$$

$$\frac{1}{2\pi}\int_V R_{11}^2 \,\mathrm{d}\boldsymbol{\eta} = \int_{-\infty}^{\infty}\int_0^{\infty}\frac{1}{\eta_\perp^2}\left[\frac{\partial}{\partial \eta_\perp}\left(\eta_\perp \frac{\partial b}{\partial \eta_\perp}\right)\right]^2 \eta_\perp \,\mathrm{d}\eta_\perp \,\mathrm{d}\eta_1 \tag{C8}$$

$$\frac{1}{2\pi}\int_V R_{11}R_{22} \,\mathrm{d}\boldsymbol{\eta} = \int_{-\infty}^{\infty}\int_0^{\infty}\left[\frac{\partial^2 b}{\partial \eta_1^2} - \frac{1}{2\eta_\perp}\left(\frac{\partial}{\partial \eta_\perp}\eta_\perp^2 a\right)\right] \times \left(\frac{\partial}{\partial \eta_\perp}\eta_\perp \frac{\partial b}{\partial \eta_\perp}\right)\mathrm{d}\eta_\perp \,\mathrm{d}\eta_1 \tag{C9}$$

Inserting Eqs. (34) and (35) into these results and integrating over $\eta_\perp$ shows that

$$\frac{\int_V R_{22}^2 \,\mathrm{d}\boldsymbol{\eta}}{2\pi L_1 L_\perp^2 \left(\widetilde{\rho u_1^2}\right)^2} = \frac{3\int_V R_{23}^2 \,\mathrm{d}\boldsymbol{\eta}}{2\pi L_1 L_\perp^2 \left(\widetilde{\rho u_1^2}\right)^2} + \mathcal{O}(\varepsilon^2) = \frac{3}{4}r^2 \int_{-\infty}^{\infty}\int_0^{\infty}\left(\tilde{\eta}_\perp \frac{\partial D}{\partial \tilde{\eta}_\perp}\right)^2 \tilde{\eta}_\perp \,\mathrm{d}\tilde{\eta}_\perp \,\mathrm{d}\tilde{\eta}_1 + \mathcal{O}(\varepsilon^2) \tag{C10}$$

$$\frac{\int_V R_{12}^2 \,\mathrm{d}\boldsymbol{\eta}}{2\pi L_1 L_\perp^2 \left(\widetilde{\rho u_1^2}\right)^2} = \mathcal{O}(\varepsilon^2) \tag{C11}$$

$$\frac{\int_V R_{11}^2 \,\mathrm{d}\boldsymbol{\eta}}{2\pi L_1 L_\perp^2 \left(\widetilde{\rho u_1^2}\right)^2} = \frac{1}{8}\int_{-\infty}^{\infty}\int_0^{\infty}\bar{B}^2 \tilde{\eta}_\perp \,\mathrm{d}\tilde{\eta}_\perp \,\mathrm{d}\tilde{\eta}_1 + \mathcal{O}(\varepsilon^2) \tag{C12}$$

$$\frac{\int_V R_{11}R_{22} \,\mathrm{d}\boldsymbol{\eta}}{2\pi L_1 L_\perp^2 \left(\widetilde{\rho u_1^2}\right)^2} = \frac{r}{2}\int_{-\infty}^{\infty}\int_0^{\infty}\bar{B}\left(\frac{\partial}{\partial \tilde{\eta}_\perp}\tilde{\eta}_\perp^2 D\right)\mathrm{d}\tilde{\eta}_\perp \,\mathrm{d}\tilde{\eta}_1 + \mathcal{O}(\varepsilon^2) \tag{C13}$$

where we have put

$$\bar{B} \equiv -\frac{1}{\bar{\eta}_\perp}\frac{\partial}{\partial \bar{\eta}_\perp}\left(\bar{\eta}_\perp \frac{\partial B}{\partial \bar{\eta}_\perp}\right) \tag{C14}$$

and r is defined by Eq. (42).

Acknowledgments

The author thanks Abbas Khavaran and Stewart Leib for their helpful comments.

References

[1]Freund, J. B., "Noise Sources in a Low-Reynolds-Number Turbulent Jet at Mach 0.9," *Journal of Fluid Mechanics*, Vol. 438, 2001, pp. 277–305.

[2]Lilley, G. M., "On the Noise from Jets," *Noise Mechanism*, CP-131, AGARD, 1974, pp. 13.1–13.12.

[3]Balsa, T. F., Gliebe, P. R., Kantola, R. A., Mani, R., Strings, E. J., and Wong, J. C. F., II, "High Velocity Jet Noise Source Location and Reduction," Federal Aviation Administration, FAA Rept. FAA-RD-76-79, 1978.

[4]Morris, P. J., and Farassat, F., "Acoustic Analogy and Alternative Theories for Jet Noise," *AIAA Journal*, Vol. 40, No. 4, 2002, pp. 671–680.

[5]Tam, C. K. W., and Auriault, L., "Jet Mixing Noise from Fine-Scale Turbulence," *AIAA Journal*, Vol. 37, No. 2, 1999, pp. 145–153.

[6]Tam, C. K. W., "Comment on "Acoustic Analogy and Alternative Theories for Jet Noise Prediction," *AIAA Journal*, Vol. 41, No. 9, 2003, pp. 1844–1845.

[7]Morris, P. J., and Farassat, F., "Reply by the Authors to C. K. W. Tam," *AIAA Journal*, Vol. 41, No. 9, 2003, pp. 1845–1847.

[8]Goldstein, M. E., "A Generalized Acoustic Analogy," *Journal of Fluid Mechanics*, Vol. 488, 2003, pp. 315–333.

[9]Lilley, G. M., "The Radiated Noise from Isotropic Turbulence with Applications to the Theory of Jet Noise," *Journal of Sound Vibration*, Vol. 190, July 1996, pp. 463–476.

[10]Morfey, C. L., Szewczyk, V. M., and Fisher, M. J., "New Scaling Laws for Hot and Cold Jet Mixing Noise Based on a Geometric Acoustics Model," *Journal of Sound and Vibration*, Vol. 46, No. 1, 1976, pp. 79–103.

[11]Lilley, G. M., "Jet Noise: Classical Theory and Experiments," *Aeroacoustics of Flight Vehicles*, edited by H. Hubbard, Vol. 1, NASA RP-1258 and WRDC TR-90-3052, 1991, pp. 211–289.

[12]Freund, J. B., "Noise-source Turbulence Statistics and the Noise from a Mach 0.9 Jet," *Physics of Fluids*, Vol. 15, No. 6, 2003, pp. 1788–1800.

[13]Ffowcs William, J. E., "Noise from Turbulence Convected at High Speed," *Philosophical Transactions of the Royal Society of London, Series A: Mathematical and Physical Sciences*, Vol. A 225, 1963, pp. 469–503.

[14]Goldstein, M. E., and Rosenbaum, B. M., "Emission of Sound from Turbulence Converted by a Parallel Flow in the Presence of Solid Boundaries," NASA TN D-7118, Feb. 1973.

[15]Goldstein, M. E., and Rosenbaum, B., "Effect of Anisotropic Turbulence on Aerodynamic Noise," *Journal of the Acoustical Society of America*, Vol. 54, No. 3, 1973, pp. 630–645.

[16]Kerschen, E. J., "Constraints on the Invariant Function of Axisymmetric Turbulence," *AIAA Journal*, Vol. 21, No. 7, 1983, pp. 978–985.

[17]Lindborg, E., "Kinematics of Homogeneous Axisymmetric Turbulence," *Journal of Fluid Mechanics*, Vol. 302, 1995, pp. 179–201.

[18]Khavaran, A., "Role of Anisotropy in Turbulent Mixing Noise," *AIAA Journal*, Vol. 37, No. 7, 1999, pp. 832–841.

[19]Batchelor, G. K., *Theory of Homogeneous Turbulence*, Cambridge Univ. Press, London, 1953, Chap. 8.

[20]Harper-Bourne, M., "Jet Noise Turbulence Measurements," AIAA Paper 2003-3214, 2003.

[21]Lighthill, M. J., "On Sound Generated Aerodynamically: I. General Theory," *Proceedings of the Royal Society of London, Series A: Mathematical and Physical Sciences*, Vol. A 211, 1952, pp. 564–587.

[22]Lighthill, M. J., "On Sound Generated Aerodynamically: II. Turbulence as a Source of Sound," *Proceedings of the Royal Society of London, Series A: Mathematical and Physical Sciences*, Vol. A 222, 1954, pp. 1–32.

[23]Pridmore-Brown, "Sound Propagation in a Fluid Flowing Through an Attenuating Duct," *Journal of Fluid Mechanics*, Vol. 4, 1958, pp. 393–406.

[24]Morse, P. M., and Feshbach, H., *Methods of Theoretical Physics*, McGraw–Hill, New York, 1953, Chap. 7.

[25]Goldstein, M. E., *Aeroacoustics*, McGraw–Hill, New York, 1976, pp. 7–10.

[26]Pope, S. B., *Turbulent Flows*, Cambridge Univ. Press, London, 2000, p. 144.

[27]Ribner, H. E., "The Generation of Sound by Turbulent Jets," *Advances in Applied Mechanics*, Vol. 8, Academic Press, New York, 1964, pp. 104–182.

[28]Hinze, J. O., *Turbulence*, McGraw–Hill, New York, 1975, p. 52.

[29]Khavaran, A., Bridges, J., and Freund, J. B., "A Parametric Study of Fine-Scale Turbulence Mixing Noise," NASA TM-2002-211696, July 2002.

[30]Abramowitz, M., and Stegun, I., *Handbook of Mathematical Functions*, National Bureau of Standards, Washington, DC, 1965.

A. Karagozian
Associate Editor